energies

MDPI

Article

Simulation, Verification and Optimization Design of Electromagnetic Vibration and Noise of Permanent Magnet Synchronous Motor for Vehicle

Jie Xu *, Lijun Zhang, Deijian Meng and Hui Su

School of Automotive Engineering, Tongji University, Jiading District, Shanghai 201804, China
* Correspondence: jiexu1988@tongji.edu.cn; Tel.: +86-18321464896

Abstract: Aiming at the electromagnetic vibration and noise problem of an 8-pole 48-slot permanent magnet synchronous motor for a vehicle, the multi-physics coupling simulation model of the motor is introduced to optimize the rotor structure of the motor to reduce the vibration and noise of the permanent magnet synchronous motor. The effectiveness of the research method is verified by the bench test in the anechoic chamber. Finite element software was used to establish the stator core and system model considering the anisotropy of materials, and the simulation model was verified by modal experiment. For the 2in1 electric drive system, the electromagnetic-structure-acoustic multi-physics coupling noise prediction model is established. Based on the three-dimensional distributed electromagnetic force excitation, the electromagnetic radiation noise of the motor under full load acceleration is calculated, and the characteristics of electromagnetic noise are analyzed. The accuracy of the electromagnetic-structure-acoustic multi-physics coupling model of permanent magnet synchronous motor is verified by the bench test results of the anechoic chamber. By changing the angle and shape of the motor rotor, the cogging torque ripple between the stator and the rotor is reduced, and the 48th order harmonic amplitude is reduced. Finally, the optimized sample is tested on the vehicle, and the 48th order electromagnetic noise can be reduced by 5–15 dB(A). The accuracy of the electromagnetic-structure-acoustic multi-physics coupling model of permanent magnet synchronous motor is verified by the bench test results of the anechoic chamber. Therefore, the research results can be further used for the design and development of a vehicle permanent magnet synchronous motor and the research on the mechanism of electromagnetic vibration and noise.

Keywords: permanent-magnet synchronous motor (PMSM); multiphysics coupling model; vibration and noise; finite element method (FEM); bench test in anechoic chamber; rotor skewing

Citation: Xu, J.; Zhang, L.; Meng, D.; Su, H. Simulation, Verification and Optimization Design of Electromagnetic Vibration and Noise of Permanent Magnet Synchronous Motor for Vehicle. *Energies* **2022**, *15*, 5808. https://doi.org/10.3390/en15165808

Academic Editor: Wenzhe Deng

Received: 11 July 2022
Accepted: 8 August 2022
Published: 10 August 2022

1. Introduction

With lower cogging torque, better weak magnetic capability and fault tolerance, permanent magnet synchronous motors have been widely used in pure electric and hybrid main drive motors. Motor vibration noise is an important index to measure the level of motor design and manufacture, and its quality directly affects the ride comfort. Motor noise includes electromagnetic noise, mechanical noise and aerodynamic noise. Due to the wide range of motor speed and high electromagnetic order, the frequency of electromagnetic noise is very wide, which is obviously different from mechanical noise and aerodynamic noise. It is more likely to make the passengers feel restless and cause more and more complaints about the sound quality of the vehicle. Electromagnetic noise induces a low frequency vibration, and the vibration frequency is usually below 100 Hz, which is a particularly dangerous vibration frequency for humans [1]. The noise generated by the pulsation of the magnetic field in the motor gap results in the vibration of the stator, rotor and the whole motor structure. The magnitude of motor electromagnetic noise is determined by the electromagnetic load and the design parameters of the motor. Electromagnetic noise is

mainly structural noise, mainly due to the improper fit of the stator and rotor slots, stator and rotor eccentricity, or the air gap is too small and of inconsistent length, etc. The noise of the motor is a superposition of different frequencies and different sound intensity noise, and this mixed noise is even as high as 110 dB or more, which will affect the health of the operator [2]. In today's strong focus on environmental protection and health maintenance, it is particularly important to find noise sources in a timely manner and to analyze and identify noise in order to take appropriate measures to mitigate it. Therefore, the electromagnetic vibration and noise prediction modeling method and the mechanism of a permanent magnet synchronous motor is particularly important.

The intrinsic mode of a motor is the inherent vibration characteristic of a mechanical structure, and each mode order has its own specific intrinsic frequency, damping ratio and mode vibration patterns. When the motor electromagnetic force order and the modal order are the same, and the electromagnetic force frequency and the modal inherent frequency are close to each other, a smaller electromagnetic force can produce a larger vibration noise [3]. Therefore, it is important to study the effect of motor structure on the modal's inherent frequency in order to avoid the resonant frequency of the motor and suppress the motor vibration noise. The accurate modeling of the motor stator system is the key to study the electromagnetic vibration and noise, simulated and analyzed the sensitivity of anisotropic material parameters. In references [4,5], through the modal test of stator core and assembly, the key parameters were identified. The experiment results further validated that the estimated error was less than 4%. In [6], the influence of temperature on the modal frequency and damping ratio of the stator and winding is studied. The results show that there is more than six times difference in damping ratio at different temperatures. Modal frequency values vary by hundreds of Hz at different temperatures. Only a few papers have considered the influence of the core lamination structure and winding in stator modeling, and there is no effective method to identify the anisotropic parameters of the stator, and how to take into account the influence of stator winding and the silicon steel lamination structure on the vibration characteristics of the motor stator is the key to accurately establishing the finite element model of the stator structure.

The radial electromagnetic force generated by the air gap magnetic field of the permanent magnet synchronous motor acting on the stator tooth surface is the fundamental source of electromagnetic vibration noise of the permanent magnet synchronous motor. The motor is the fundamental source of the electromagnetic vibration noise. Consequently, the study of the radial electromagnetic force of permanent magnet synchro-nous motor is essential to analyze the vibration noise of permanent magnet synchronous motor. Therefore, the study of radial electromagnetic force of the PMSM is important to analyze the electromagnetic vibration noise of PMSM. In the consideration of electromagnetic force excitation research, most of the research focuses on the radial force excitation under the ideal sinusoidal current input; some literature began to consider the influence of electromagnetic force tangential force, radial force and current harmonics on the vibration noise. The traditional electromagnetic noise simulation mainly focuses on radial force and ignores the electromagnetic force component, which affects the simulation accuracy. In the literature [7], the radial electromagnetic force alone and the combined radial, tangential and axial electromagnetic force are analyzed. The results show that the tangential electromagnetic force has a certain degree of influence on the electromagnetic noise, and the motor stator model with radial, tangential and axial electromagnetic force is more realistic and reliable. In [8], the authors carried out the transient dynamics simulation of a permanent magnet synchronous motor is carried out considering the influence of radial electromagnetic force and tangential electromagnetic force on electromagnetic vibration, and the results are analyzed by frequency response [9]. The results show that the tangential electromagnetic force in the time domain makes the tangential deformation of the motor stator teeth significantly larger than the radial; in the frequency domain, the influence of the second order torque pulsation frequency, which is closely related to the tangential electromagnetic force, on the electromagnetic vibration is not negligible. In [10], the authors introduced a computational method to analyze the

effect of inverter harmonics on the vibration noise of an electric vehicle built-in permanent magnet synchronous motor over a wide speed range, derived the characteristic parameters of the electromagnetic force wave of the motor when the inverter current harmonics are supplied, analyzed the vibration noise spectral characteristics of an electric vehicle IPMSM with constant torque speed regulation and weak magnetic speed regulation, and verified the correctness of the joint simulation model by experiments.

When the motor is energized, the electromagnetic force generated by the magnetic field of the motor, which changes continuously with time and space, will act on the motor stator and rotor to form excitation, causing electromagnetic vibration and deformation of the motor, so that the motor produces electromagnetic noise. Because the electromagnetic vibration noise of the motor is the main noise source when the motor is running, it must be focused on because the electromagnetic vibration noise of the motor is the main source of noise during the operation of the motor; it must be focused and studied in detail. Some studies focus on analytical or quasi-analytical methods [4,11], and increasingly mature methods such as the finite element and boundary element have also started to be widely applied to the prediction of motor electromagnetic vibration noise. In [11], the authors proposed a quasi-analytical method for the vibration noise of a permanent magnet-assisted synchronous reluctance motor, which can analyze the effect of different rotor topologies of the motor on the vibration noise. In [12], the electromagnetic finite element model, kinetic finite element model and acoustic boundary element model of the generator were established for the electromagnetic noise problem existing in a type of vehicle claw-pole generator, and the numerical simulation with multi-physics field coupling was carried out to compare the average sound pressure level on the test hemisphere obtained from the simulation and experiment, respectively, and it was found that they were in good agreement, indicating that the numerical simulation method has high accuracy. In [13], the authors introduced a method to calculate the electromagnetic force and electromagnetic noise of a motor using multi-physics field coupling, firstly calculating the electromagnetic force using electromagnetic software, and after that mapping the electromagnetic force to the corresponding structural grid to calculate the vibration response, and finally calculating the motor radiation noise using an acoustic solver, finally verifying the effectiveness of the method using experimental results, which has now been widely applied to the study of electromagnetic vibration noise calculation of motors.

In terms of motor vibration and noise suppression measures, this mainly includes changing the inclined pole mode, the structure of the magnetic isolation bridge, the structure assembly mode and the current compensation. In [14], in order to weaken the electromagnetic force harmonics caused by tooth harmonics and thus effectively suppress the electromagnetic noise of the motor, the analytical equation of radial electromagnetic force waves of the rotor's segmented diagonal poles is derived, the suppression mechanism of segmented diagonal poles on electromagnetic noise of permanent magnet synchronous motor is analyzed, and the relationship between the number of different diagonal pole segments and the weakened tooth harmonic order is discussed. For the V-rotor permanent magnet motor for 30 kW electric vehicle drive, an optimization scheme using a new magnetic isolation bridge is proposed in the literature [15] and simulated under several characteristics, and then the feasibility and validity are verified through prototype experiments In [16], the authors used an experimental method to analyze the effect of the friction damping coefficient between the water jacket and the casing on the radiated noise of the motor, and the results showed that changing the friction coefficient between the water jacket and the casing can effectively improve the motor noise problem. In [17], the authors proposed a method for fractional-slot permanent magnet synchronous motors to inject a certain compensation current into the stator winding to cancel the radial force harmonics with the lowest modulus and thus suppress the electromagnetic vibration of fractional-slot motors. In [18], the authors proposed a stator tooth top offset structure to weaken the larger radial electromagnetic force on the stator teeth based on the distribution law of the radial electromagnetic force on the stator teeth, and this measure not only weakened the radial

electromagnetic force with larger amplitude but also reduced the torque fluctuation. At present, the segmented rotor pole-shifting has been widely used in practical production. Many experts and scholars in China and abroad have also undertaken in-depth research and fruitful work on the influence of segmented rotor pole-shifting on the electromagnetic performance of a motor such as cogging torque and axial force [19]. On the one hand, the segmented rotor pole-error weakens the torque ripple and cogging torque of the permanent magnet synchronous motor, thereby improving the noise characteristics of the permanent magnet synchronous motor [20]. On the other hand, the rotor segment misalignment of the permanent magnet synchronous motor also affects the radial electromagnetic force of the motor, which is another main reason why the rotor segment misalignment affects the electromagnetic vibration and the noise of the motor [21]. Many scholars have carried out a lot of research and analysis on the influence of rotor segment misalignment on motor vibration and noise. However, the analytical method based on in-depth analysis of rotor piecewise pole error on permanent magnet synchronous motor radial electromagnetic force and vibration noise has not been reported.

In order to accurately predict the electromagnetic vibration and noise of a permanent magnet synchronous motor and to optimize it for 48th order electromagnetic noise, this paper conducts a study on an 8-pole 48-slot vehicle permanent magnet synchronous motor. In Section 2, a stator core and stator system model considering material anisotropy characteristics is established, the sensitivity of anisotropic material parameters is analyzed, and the simulation model is verified using exciter modal knockout experiments. In Section 3, a coupled electromagnetic-structural-acoustic multi-physical field model is established for the 2in1 system of a permanent magnet synchronous motor and drive bridge, based on a three-dimensional distributed electromagnetic force excitation considering radial and tangential forces. In Section 4, the mechanism of 48th order noise peak point generation near 2000 rpm is elucidated, and the suppression effect of 48th order electromagnetic noise is achieved by optimizing different diagonal pole shapes of the rotor, and the results of the anechoic chamber bench experiments are used to verify the effectiveness of the PM synchronous motor EM-structure-acoustics multi-physics field coupling. The effectiveness of the model and the optimization scheme is verified. Finally, the concluding remarks are presented in Section 5.

2. Stator Anisotropy Modeling and Modal Analysis

2.1. Study of Stator Anisotropy Characteristics

In this paper, the motor adopts a hairpin flat winding type, and its basic parameters are shown in Table 1. The stator system is mainly composed of the stator core and winding: the stator core is made of multilayer silicon steel sheets laminated in the axial direction, and the winding is made of flat wire winding of hairpin type. The axial laminated structure of the stator core leads to different mechanical properties along different directions, and the material parameters show obvious orthogonal anisotropy, the accurate modeling of which directly affects the simulation accuracy of the electromagnetic vibration noise of the motor.

Table 1. Parameters of permanent synchronous electrical motor.

Parameters	Value	Parameters	Value
Peak power	100 kW	Peak torque	300 Nm
Rated power	45 kW	Rated torque	120 Nm
Number of stator skew	6	Stator skew type	piecewise linearity
Stator skew angle	0.9°	Winding type	hairpin
Slot	48	pole	8

In the finite element modeling of the motor structure, the stator core lamination structure and winding type cannot be modeled in detail according to the actual shape structure, so the stator core and winding need to be treated in an equivalent way. For the stator core, a solid model is established according to the actual model dimensions considering the lamination coefficient, as shown in Figure 1a, and the core material is set

up with density according to the principle of mass equivalence, and different moduli of elasticity and shear modulus are assigned to the core material in each direction. For the stator system, the hairpin flat wire winding is embedded in the stator tooth slot, and the stator core is divided into two parts, the stator yoke part and the stator tooth part, during the equivalence, as shown in Figure 1b. The material parameters of the stator yoke are kept the same as those of the stator core, and the winding mass is increased to the stator tooth part according to the principle of mass equivalence, and the parameters of the elastic modulus and shear modulus of the stator tooth material are adjusted.

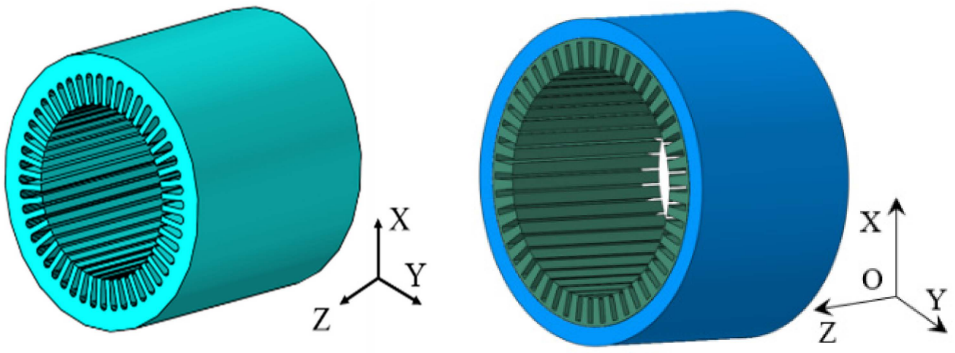

(**a**) (**b**)

Figure 1. Equivalent finite element model of stator core and stator system. (**a**) stator core; (**b**) stator system.

For the stator core structure shown in Figure 1a, the stator material anisotropy is considered in the modeling, and the anisotropic material requires a total of nine material constants in three orthogonal symmetry planes to be defined. In the XOY plane, the material is isotropic, and the material parameters are the same as those of the single-layer silicon steel sheet; in the XOZ and YOZ planes, the material is anisotropic, and the material anisotropy parameters are the same in the corresponding directions in both planes; the effect of the laminated structure on the Poisson's ratio of the material is ignored. Therefore, the relationships of the nine material parameters of the stator core are: Poisson's ratio, $\nu_{XY} = \nu_{XY} = \nu_{XY} = 0.29$ [22]; Young's modulus, $E_X = E_Y$, E_Z; shear modulus, G_{XY}, $G_{XZ} = G_{YZ}$. Through the above relationships, it can be seen that there are only four variables, E_X (E_Y), E_Z, G_{XY} and G_{XZ} (G_{YZ}), among the nine material parameters of the stator core. In order to accurately define the anisotropic material parameters in the simulation model for comparison with the modal test results, the modal analysis was performed with different values of E_X (E_Y), E_Z, G_{XY} and G_{XZ} (G_{YZ}) variables, respectively, and the values of the variables are shown in Table 2. The modal results obtained from the simulation are shown in Figures 2 and 3, respectively.

Table 2. Anisotropic material parameter values.

Parameter	Case 1	Case 2	Case 3	Case 4
E_X, E_Y	200 GPa	150 Gpa	100 GPa	50 GPa
E_Z	200 GPa	150 GPa	100 GPa	50 GPa
G_{XY}	80 GPa	60 GPa	40 GPa	20 GPa
G_{XZ}, G_{YZ}	80 GPa	60 GPa	40 GPa	20 Gpa

In Figures 2 and 3, m represents the axial modal order, when m = 0 the stator vibrates in phase along the axial direction, and m = 1 the stator vibrates in anti-phase at both ends of the axial direction. n represents the radial modal order [9]. As can be seen from Figure 2, when the motor stator axial modal order m = 0, the two variables E_X (E_Y) and G_{XY} among the anisotropic parameters have a large effect on the radial modal frequency n (n = 2, 3, 4, 5, 6) of the motor stator core, while E_Z and G_{XZ} (G_{YZ}) have a negligible effect on the modal frequency. As can be seen from Figure 3, when the stator axial mode order m = 1, the three variables E_X (E_Y), G_{XY} and G_{XZ} (G_{YZ}) among the material anisotropy parameters have a greater effect on the core radial mode frequency n (n = 2, 3, 4, 5, 6),

especially the higher order n, which is more sensitive to the changes of parameters E_X (E_Y) and G_{XY}, while the effect of E_Z on the stator core radial mode frequency is relatively smaller. The sensitivity analysis of the anisotropic material parameters of the stator yoke and stator teeth is the same as that of stator core, and the effect of anisotropic material parameters on the modal frequency of stator system is the same as that of the stator core.

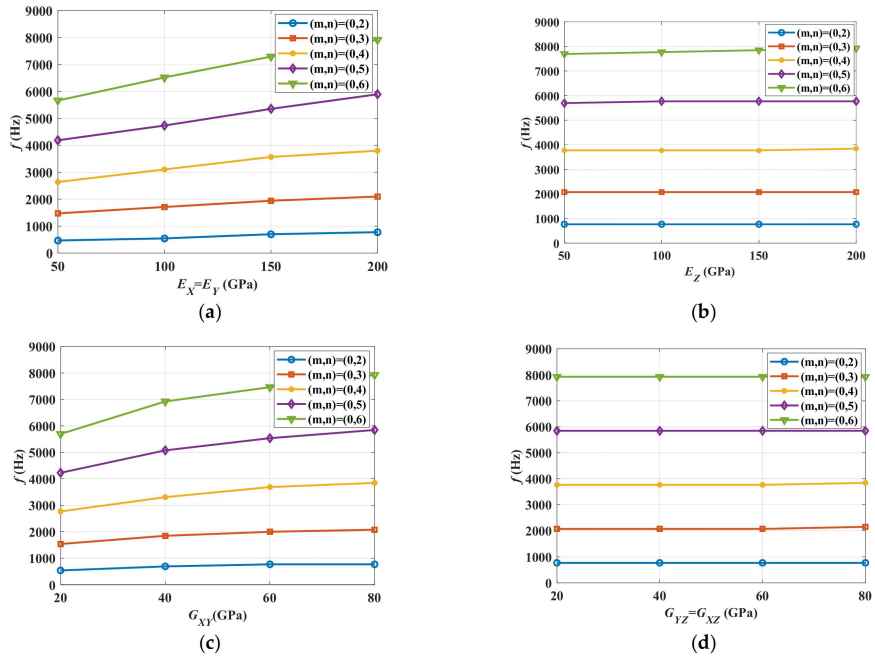

Figure 2. Anisotropic material property influence on stator core modal frequency of m = 0. (**a**) Effects of E_X and E_Y; (**b**) Effects of E_Z; (**c**) Effects of G_{XY}; (**d**) Effects of G_{YZ} and G_{XZ}.

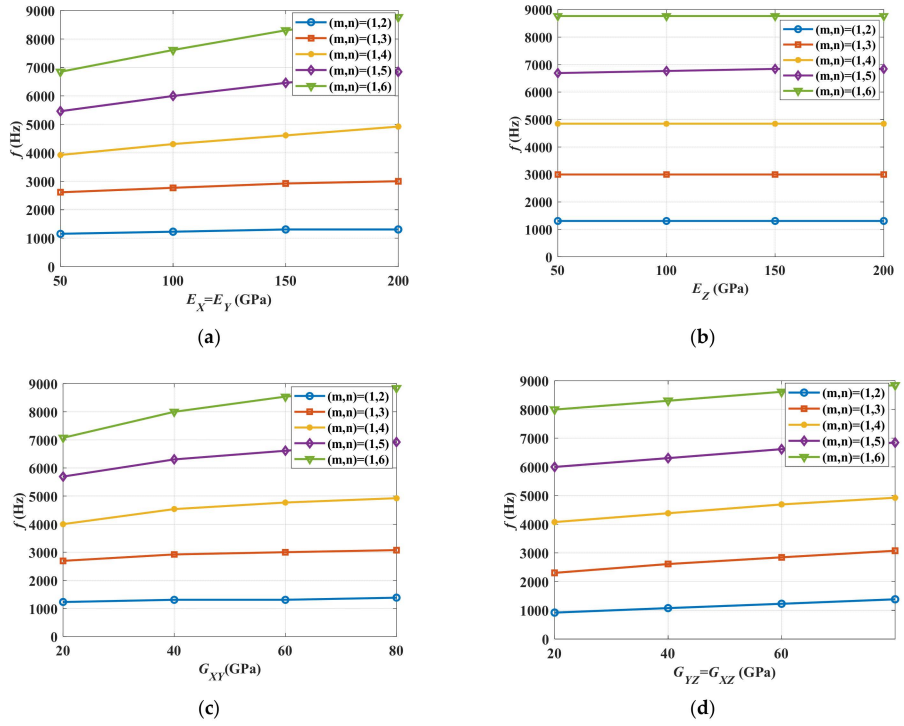

Figure 3. Anisotropic material property influence on stator core modal frequency of m = 1. (**a**) Effects of E_X and E_Y; (**b**) Effects of E_Z; (**c**) Effects of G_{XY}; (**d**) Effects of G_{YZ} and G_{XZ}.

2.2. Model Test

In order to study the anisotropic material parameters of the stator core and stator system, the stator core and stator system modal experiments were carried out respectively, and the test setup is shown in Figure 4. In the experiment, the stator core and stator system are excited by the shaker, and the vibration signal is obtained from the measurement points using vibration sensors. The results of the stator core and stator system modal experiments are shown in Table 3.

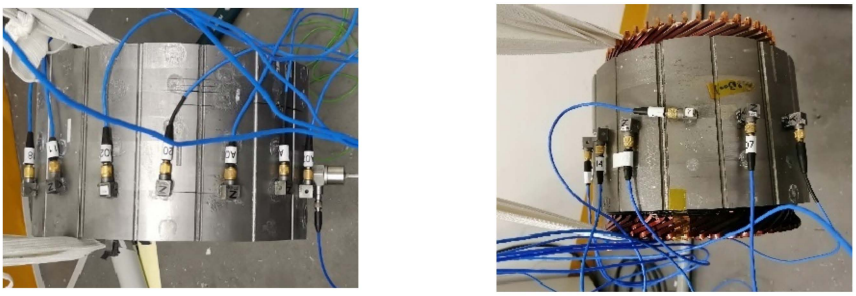

(**a**) (**b**)

Figure 4. Stator core and stator system modal test. (**a**) Modal experiment of stator core; (**b**) Modal experiment of stator system.

Table 3. Modal test results.

Modal Order		Modal Frequency/Hz	
Axial	**Radial**	**Stator Core**	**Stator System**
m = 0	n = 2	763.2	689.3
	n = 3	2070.7	1823.8
	n = 4	3754.5	3267.9
m = 1	n = 2	814.5	1060.3
	n = 3	2160.0	1879.0
	n = 4	3824.1	3747.9

2.3. Comparison of Simulation and Test Results

Based on the modal simulation results, the three variables E_X (E_Y), G_{XY} and G_{XZ} (G_{YZ}) are used as the adjustment parameters, and the measured modal results are used as the optimization target. The equivalent anisotropic material parameters of the stator core and stator system are obtained, and the corresponding simulation and measured modal frequency comparison results are shown in Table 4. When considering the anisotropic material parameters of the stator core and the stator system, the error between the simulation and actual measurement of the core modal frequency is 2%. The modal frequency simulation and actual measurement error of the stator system is within 1%.

Table 4. Simulation and test modal results.

m = 0		Model Frequency/Hz		
		n = 2	**n = 3**	**n = 4**
Stator Core	Simulation	762.7	2045.3	3719.7
	Test	763.2	2070.7	3754.5
	Relative Error	0.06%	1.24%	0.93%
Stator System	Simulation	688.7	1812.4	3273.7
	Test	689.3	1823.8	3267.9
	Relative Error	0.08%	0.63%	0.17%

3. Simulation Analysis of Electromagnetic Vibration and Noise of PMSM

3.1. Simulation Workflow

The key process of electromagnetic vibration noise multi-physics field modeling and simulation of motors is as follows:

Step 1: Firstly, ignoring the effect of inverter pulse width modulation, an electromagnetic finite element model of an 8-pole 48-slot permanent magnet synchronous motor is established. Considering the inverter output current fundamental wave under each operating condition, the electromagnetic force results on the stator tooth surface and tooth slot surface are calculated, including radial force and tangential force. Further, based on the double Fourier transform results of the air gap force density between the stator and rotor, the characteristic parameters of the electromagnetic force wave and the main harmonic sources are analyzed [14,23].

Step 2: Based on the two-dimensional electromagnetic force results for each segment calculated in step (1), the two-dimensional electromagnetic force results are expanded into three-dimensional electromagnetic forces and the six three-dimensional electromagnetic force results are combined into an overall electromagnetic force.

Step 3: Consider the anisotropic material parameter characteristics of the stator system, establish the finite element model of the 2in1 system of motor and drive bridge, and calculate the modal results of the 2in1 system.

Step 4: The electromagnetic force is transferred from the electromagnetic grid to the structural grid by controlling the spatial position of the three-dimensional electromagnetic grid and the structural grid of the stator system to keep the same position. Calculating the system vibration response results using the modal superposition method based on the overall electromagnetic force results synthesized in step (2) and the system modal results in step (3).

Step 5: Finally, the system shell surface vibration response results are mapped to the inner surface of the acoustic mesh, and the system acoustic radiation results are calculated using the acoustic finite element method.

3.2. Noise Analysis of PMSM

Acoustic measurement points were arranged at 1 m each above, in front of, behind, and on the left and right side of the electric driving system housing surface, and the reflection effect of ground on sound propagation was considered to simulate and evaluate the acoustic performance of the motor under peak torque operating conditions.

Taking the 1 m acoustic measurement point in the rear as an example, the acoustic results of this measurement point are shown in Figure 5. From Figure 5a, it can be seen that based on the eighth order and its eighth integer multiple orders, the overall contribution to the sound pressure is larger, and there are more obvious resonance bands near 4000 Hz and 8000 Hz. From the comparison of the overall sound pressure and each order in Figure 5b, it can be seen that the 48th order noise has the largest contribution to the overall sound pressure in the full speed range. In the range of 0 to 7000 rpm, the 48th order noise amplitude increases with the increase of speed. There are obvious peak points near 2000 rpm and 7000 rpm. In the range of 7000 rpm to 16,000 rpm, the 48th order noise amplitude decreases with the increase of speed. In the range of 0 to 7000 rpm, the overall 48th order noise amplitude increases with the increase of speed, and there are obvious peak points near 2000 rpm and 7000 rpm, and in the range of 7000 rpm to 16,000 rpm, the overall 48th order noise amplitude decreases with the increase of speed.

Viewing the simulation results of the five acoustic measurement points at 1 m, the conclusions are consistent with the acoustic measurement points at the rear 1 m, where the 48th order noise summary results of the five acoustic measurement points are shown in Figure 6. It can be seen that in the range of 0 to 7000 rpm, the overall 48th order noise amplitude increases with the increase of speed, and there are more obvious peak points near 2000 rpm and 7000 rpm; in the range of 7000 rpm to 16,000 rpm, the overall 48th order noise amplitude decreases with the increase of speed.

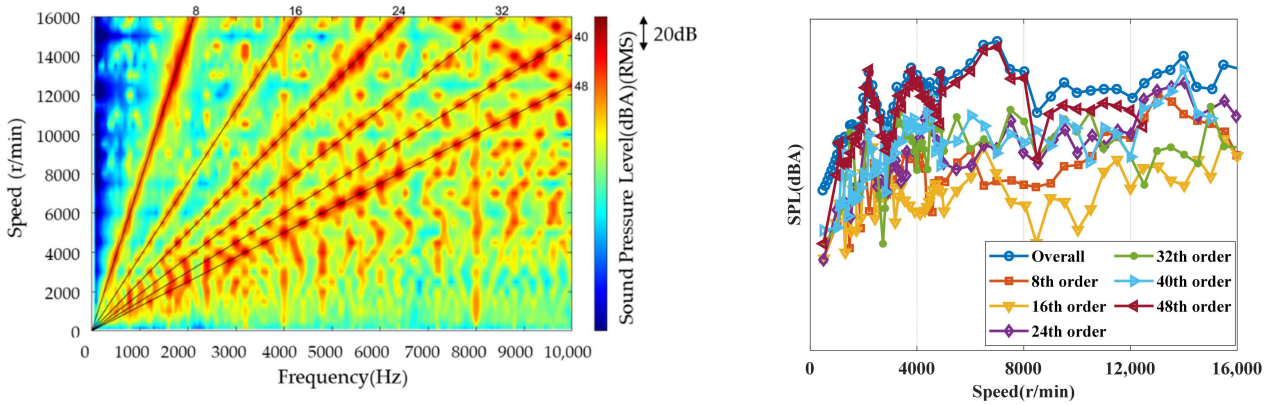

Figure 5. Rear 1 m acoustic measurement point location noise results. (**a**) Microphone sound pressure level colormap results; (**b**) Overall level and order cut level of Microphone sound pressure.

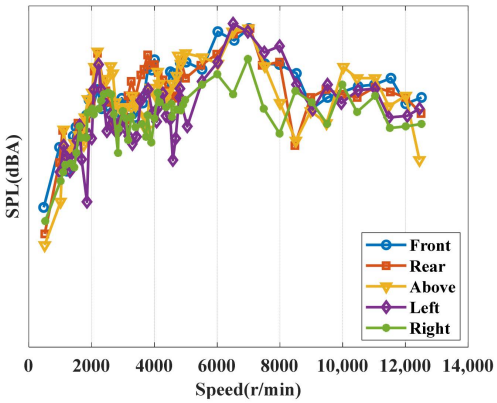

Figure 6. Simulation results of five microphones at a distance of 1 m.

3.3. Verification of Prototype Experiment

In the anechoic chamber, the electromagnetic noise of the permanent magnet synchronous motor was tested under full-load acceleration conditions, and the LMS SCADAS SCM205 multi-channel data acquisition equipment was used at the test front end, and the microphones were arranged in the 2in1 system near the top, front, rear, left and right side of the shell surface at 1 m. The overall experimental arrangement is shown in Figure 7.

Taking the microphone measurement point at 1 m in the rear as an example, the simulated and tested 48th order comparison results are shown in Figure 8. It can be seen that in the speed range from 0 to 7000 rpm, the simulated and tested 48th order noise amplitude generally increases with the increase of speed, and there are obvious peak points near 2000 rpm and 7000 rpm in both simulated and tested results; in the speed range from 7000 to 13,000 rpm, the 48th order noise amplitude generally decreases with the increase of speed. The simulated and tested results are in good agreement in the full speed range, thus verifying the effectiveness of the coupled electromagnetic-structural-acoustic multi-physical field simulation of the permanent magnet synchronous motor established in this paper. In the speed range from 0 to 7000 rpm, the overall 48th order noise amplitude increases with increasing speed, and there are obvious peak points near 2000 rpm and 7000 rpm; in the speed range from 7000 to 13,000 rpm, the overall 48th order noise amplitude decreases with increasing speed. This result further verifies the validity of the multi-physics field coupling model.

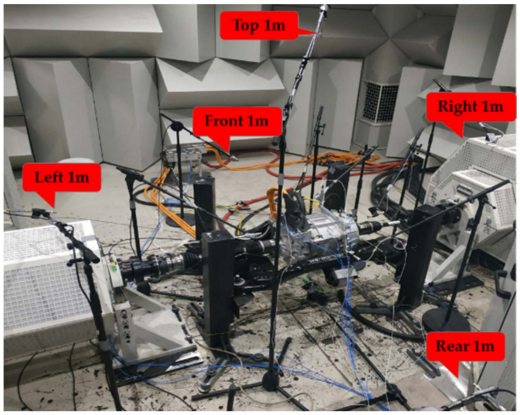

Figure 7. Noise Test of Permanent Magnet Synchronous Motor.

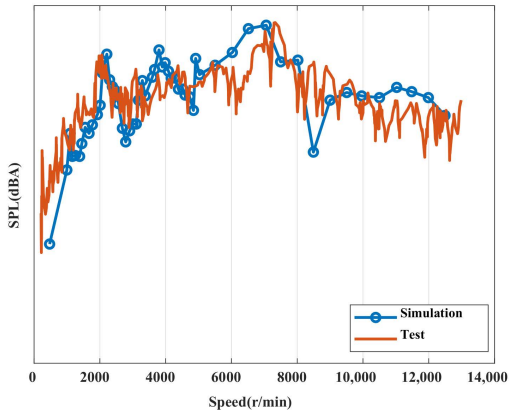

Figure 8. Simulation and test comparison of rear 1 m.

4. Noise Optimization of Permanent Magnet Synchronous Motor

4.1. 48th Order Noise Analysis

When we were developing the 2in1 electric drive system that is the subject of this paper, we found that the prototype vehicle equipped with this assembly had a significant whine phenomenon of the permanent magnet synchronous motor at the vehicle speed of 10–50 km/h. At the same time, according to Figure 5b, it can be seen that in the speed range of 0–16,000 rpm, 48th order noise has a greater contribution to the overall sound pressure, and there are obvious peak points near 2000 rpm and 7000 rpm. This paper does not do much analysis on other low-order noises, mainly because the low-order noise frequencies are relatively low and a large part of them are attenuated by the powertrain mounts, so they have less impact on the driver. In addition, due to the low speed of the vehicle, the 48th order noise frequency is right in the sensitive area of the human ear, so this paper analyzes the problem with a focus on reducing the 48th order noise.

To address the problem of the peak electromagnetic noise near 2000 rpm in the simulated and measured 2in1 system (the electromagnetic noise in this speed range is very likely to cause passenger irritation and customer complaints), an Operational Deflection Shape (ODS) test experiment was designed to investigate the mechanism of this problem. Forty-four vibration sensors were placed on the surface of the 2in1 system, and vibration tests were conducted under full-load acceleration conditions. The vibration results under the acceleration condition were extracted and the ODS test results at the 48th order frequency (1600 Hz) under the 2000 rpm speed condition were shown in Figure 9, which shows that the 2in1 system exhibits the overall torsional vibration at this frequency, especially the maximum amplitude of torsional vibration on the drive axle side. Correspondingly, the simulation results of ODS at the 48th order corresponding frequency for this speed condition are shown in Figure 10, which shows that the overall torsional vibration with the

largest amplitude of torsional vibration on the drive axle side is shown, and this conclusion is consistent with the ODS test results.

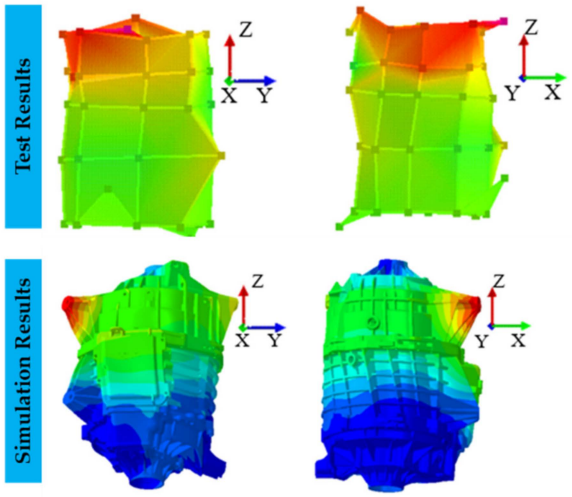

Figure 9. ODS simulation and test results.

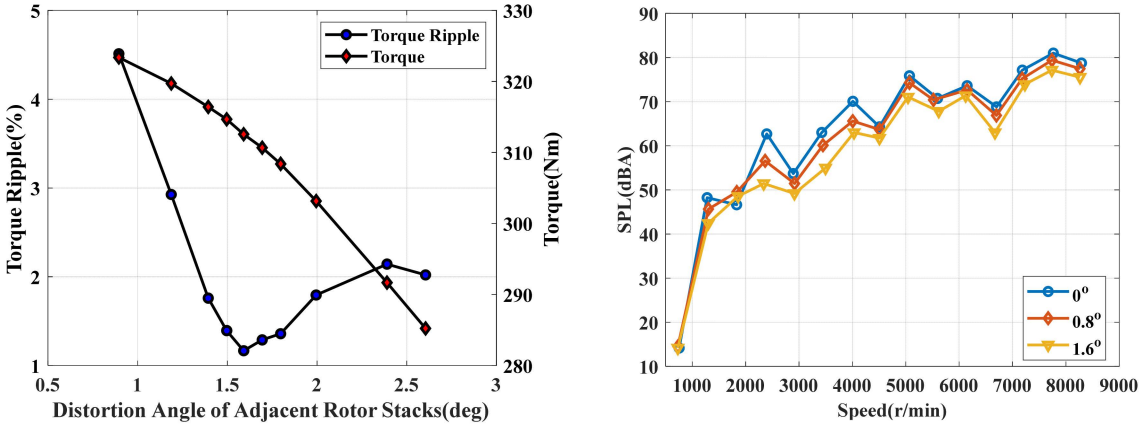

(**a**) (**b**)

Figure 10. Optimization results of different skew angles. (**a**). Comparison of torque amplitude and torque ripple at different skew angles; (**b**) Comparison of sound pressure levels at different skew angles.

The 48th order involves many factors, such as mechanical structure, torque ripple, electromagnetic excitation, structural mode and so on. There is cogging torque in the structure of the permanent magnet motor, that is, the torque generated by the interaction between the permanent magnet of the motor winding and the stator core. The tangential component of this part of the electromagnetic force will produce the order noise related to the number of slots and the pole logarithm parameters of the motor, which will lead to the fluctuation of the motor speed, meaning that the motor cannot operate smoothly. Therefore, one of the most effective methods for reducing the electromagnetic noise of the permanent magnet motor is to reduce the cogging torque ripple.

There has been a large amount of literature discussing and deriving the formulae for calculating the cogging torque. Of the two most commonly used, one is the formula for calculating the harmonic number of the cogging torque, which can be expressed as

$$N = 2pQ/N_m k(k = 1, 2, 3 \cdots) \quad (1)$$

where, N is the number of cogging torque harmonics, p is the number of motor rotor pole pairs, Q is the number of motor stator slots, N_m is the maximum convention of the number of pole pairs and slots. The permanent magnet synchronous motor studied in this paper is

the more common 8-pole 48-slot winding, so when the motor parameters are brought into the equation, the resulting calculated slot torque causes the maximum 48th order noise, which is in perfect agreement with the test results.

Another general empirical formula for the calculation of cogging torque is as follows.

$$T_{eog} = \sum_{i=1}^{\infty} K_{sk} T_i \sin\left(iN_p\theta + \varphi_i\right) \tag{2}$$

where, T_i, φ_i, are the amplitude and phase angle of the ith order cogging torque harmonic, N_p is the least common multiple of the number of stages and slots of the motor rotor, θ is the angle between the centerline of the motor stator teeth and the centerline of the permanent magnet, K_{st} is the slope slot factor. Since the original design of this motor rotor is six stacks of "one" type, this design will lead to the superposition of six stacks of electromagnetic force at the same time, and the instantaneous output electromagnetic force and slot torque will be six times of the single rotor stack, so the electromagnetic noise will be prominent and obvious.

4.2. Electromagnetic Noise Optimization

For the motor rotor designed by multi-stack rotor, it is one of the most effective methods to reduce the cogging torque of the motor by tilting a certain mechanical angle of the rotor. When the tilt angle is small, the total output of the electromagnetic force can be maintained, which has a small impact on the fundamental wave of the electromagnetic torque. However, the instantaneous output of each electromagnetic force staggers at a certain angle, which will reduce the amplitude of each harmonic of the electromagnetic torque of the motor, and then reduce the electromagnetic noise.

The electromagnetic simulation model is established using Ansys Maxwell software to analyze the transient magnetic field distribution and the electromagnetic force applied to the stator tooth surface. Since the tooth slot torque is caused by the tangential component of the electromagnetic force, the Fourier transform of the tangential electromagnetic force can be used to obtain the amplitude of the tangential electromagnetic force at different frequencies or different orders. In this paper, the rotor skew angle is optimized to achieve the purpose of suppressing 48th order electromagnetic noise. Therefore, we analyze the changes of torque amplitude and torque fluctuation of the motor with three different oblique angles of 0.8°, 1.2° and 1.6°, as shown in Figure 10a. The results show that the peak torque can be guaranteed to the maximum extent when the angle is 0.8°. When the oblique angle is 1.6°, the minimum torque ripple of the motor is 1.15%. The results of the electromagnetic force scheme with different oblique angles and the relevant information of the shell mode are imported into LMS Virtual Lab software for sound field simulation analysis. The order of acoustic simulation results is extracted, and the 48th order electromagnetic noise simulation results are shown in Figure 10b. It can be seen that the scheme with 1.6° has the lowest sound pressure level and the best optimization effect.

At the same time, the samples of rotors with different oblique angles are made, and the vehicle bench test in the semi-anechoic chamber is carried out. The test results are shown in Figure 11. From the bench test results, it can be concluded that the 1.6° skew angle indeed significantly reduces the 48th order noise.

The above tests have proved that the tilt of each segment of the rotor at a certain angle can effectively reduce the 48th order electromagnetic noise caused by the cogging torque. However, in the test, it was found that the 48th order electromagnetic noise has a significant peak when the motor is accelerated to 2000 revolutions, which can be about 5–10 dB (A) higher than the surrounding speed. This phenomenon is studied from the aspect of the electromagnetic excitation source. In the aspect of electromagnetic excitation, it is introduced that a part of the 48th order electromagnetic noise can be reduced by changing the angle of the rotor skew. However, after the rotor tilts at a certain angle, the tangential direction of the electromagnetic force is transformed by Fourier transform to

extract the 48th order electromagnetic force, and the rotor segmentation analysis is carried out by randomly intercepting three times: t1, t2 and t3, in the 48th order electromagnetic force cycle. The results show that the unbalanced electromagnetic force exists in the 48th order at three times, as shown in Figure 12. That is to say, the six-stage laminated rotor itself always outputs a 48th order torsional electromagnetic force, coupled with the addition of torsional modes in the transmission process, which leads to the increase of 48-order noise when the bridge is accelerated to 2000 rpm.

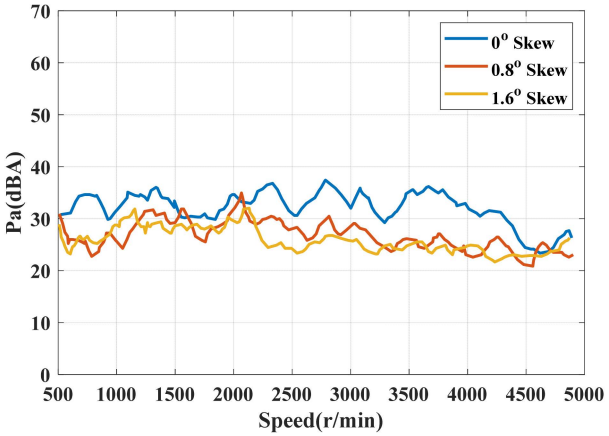

Figure 11. 48th order noise test results with different skew angles.

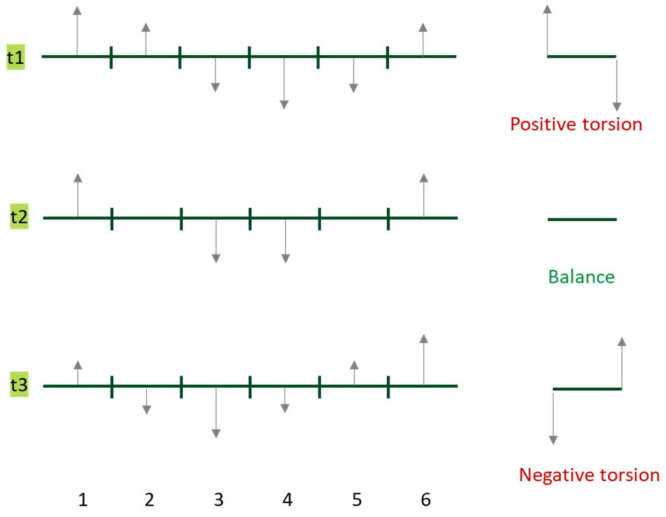

Figure 12. 48th order tangential electromagnetic force distribution of a 'liner' shape structure.

In terms of the structural mode, the natural frequency can be improved by increasing the stiffness of the stator and assembly and reducing the mass. The increase of natural frequency means greater background noise masking and smaller structural vibration response. However, improvements are usually limited. Reducing excitation is a more effective and radical method to solve the problem. The data show that changing the position relationship between each stack of the rotor is also a good method to reduce the electromagnetic noise. Generally, the shape of the segmented rotor is inclined 'liner' shape, 'V' shape and 'Z' shape. Due to the design requirements and manufacturing precision problems, the 'Z' shape rotor structure is rarely used in automobile production projects. Therefore, we analyze the 48th order electromagnetic force of the 'V' shape structure at different times, which is the same as that of the 'liner' shape structure, and the results are shown in Figure 13. The results show that there is only equilibrium force or upper and

lower electromagnetic force in the 48th order at three moments, and there is no torsional force, so the torsional vibration of the motor can be effectively suppressed.

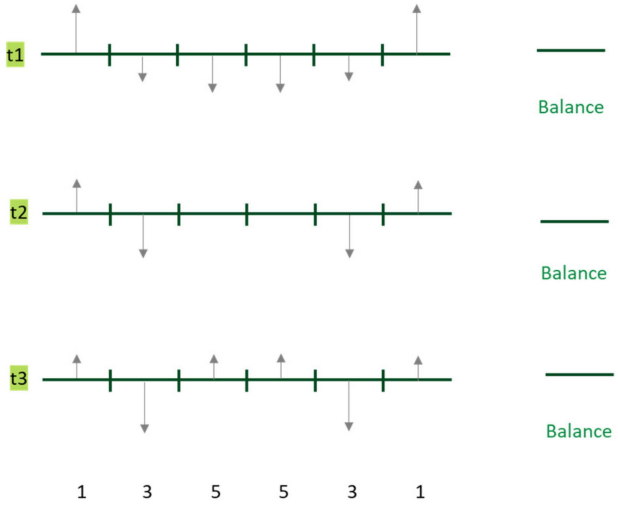

Figure 13. 48th order tangential electromagnetic force distribution of 'V' shaped structure.

Combined with the analysis of the 48th order noise from the previous rotor skew angle, we used the previous 1.6° skew angle scheme of each stacked piece to process and manufacture the 1.6° electric drive sample of 'V' shape, and compared it with the previous original 'liner' shape sample and the 1.6° skew angle sample. The results are shown in Figure 14. It can be seen from the results that the 48th order noise level of 1.6° with the 'V' shape is the lowest under the commonly used 5500 rpm of the motor. Due to the absence of torsional electromagnetic force at 2000 rpm, the acceleration noise linearity is more peaceful.

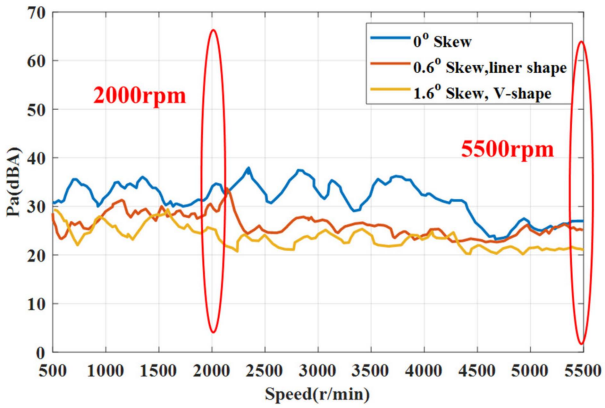

Figure 14. Noise result of different rotor structures.

5. Conclusions

(1) For the complex structure of the stator core and stator subsystem, when considering the anisotropic material parameters of the stator core and stator subsystem to establish the system equivalent model, the error of modal frequency simulation and measurement of the core is within 2%. The error of modal frequency simulation and measurement of the fixed subsystem is within 1%, and this method can accurately simulate the modal frequency of the stator system.

(2) A coupled electromagnetic-structural-acoustic multi-physical field model for electromagnetic vibration noise prediction of a permanent magnet synchronous motor is established to simulate and predict the acoustic results of the motor under full load conditions. For the 48-slot 8-pole PMSM, the frequency of radial electromagnetic force is $f_1 = 2kpf_0$, $k = 0, 1, 2, 3 \cdots$, which means that the basic order eight of the motor and its

eighth integer multiple order noise contribute the most to the overall noise. This can be seen from the simulation results, and the 48th order noise of the motor almost in the full speed region for the overall sound pressure level contribution are larger. The eighth order electromagnetic force wave, which should be larger, is lower in the simulation and test due to its lower frequency and the low frequency blocking effect of the electric vehicle suspension system. Finally, the accuracy of the simulation model was verified by using the results of the bench acoustic test in the semi-anechoic chamber.

(3) The overall sound pressure level and the 48th order sound pressure level both have obvious peak points around 2000 rpm at low speed. The ODS test shows that the 2in1 system at the 48th order frequency (1600 Hz) at 2000 rpm is characterized by the overall torsional vibration, especially the highest amplitude of torsional vibration on the drive axle side. Correspondingly, the simulation method obtained the same overall torsional vibration with the highest amplitude of torsional vibration on the drive axle side at the 48th order corresponding frequency under the speed condition. At this time, the overall torsional vibration of the system occurs, resulting in a larger amplitude and thus a larger 48th order amplitude.

(4) The 48th order electromagnetic noise of the motor can be effectively reduced by optimizing the rotor skew angle and shape. The simulation and experiment are carried out for the V-shaped skewed rotor with the sampling rotor skew angle of 1.6°. It can be found that the noise is significantly reduced in the range of 2000 rpm and low speed. The noise is reduced by nearly 10 dB, especially at 2000 rpm.

Author Contributions: Writing—original draft preparation, J.X.; data curation, J.X.; software, J.X. and H.S.; writing—review and editing, L.Z. and D.M.; supervision, D.M. All authors have read and agreed to the published version of the manuscript.

Funding: This research was funded by Chongqing Technology Innovation and Application Development Special Project, grant number cstc2020jscx-dxwtBX0031.

Institutional Review Board Statement: Not applicable.

Informed Consent Statement: Not applicable.

Data Availability Statement: The data presented in this study are available upon request from the corresponding author.

Conflicts of Interest: The authors declare that they have no conflict of interest.

References

1. Stosiak, M.; Karpenko, M.; Deptuła, A. Coincidence of pressure pulsations with excitation of mechanical vibrations of hydraulic system components: An experimental study. *Cogn. Sustain.* **2022**, *1*, 2. [CrossRef]
2. Wu, W.H.; Chen, J.F. Introduction to the formation of motor noise and practical control methods. *Dev. Innov. Mach. Electr. Prod.* **2003**, *3*, 45–47.
3. Yin, H.; Zhang, X.; Ma, F.; Gu, C.; Gao, H.; Wang, Y. New equivalent model and modal analysis of stator core-winding system of permanent magnet motor with concentrated winding. *IEEE Access* **2020**, *8*, 78140–78150.
4. Zuo, S.G.; Zhang, Y.; Yan, J. Optimization of vibration and noise in permanent magnet synchronous motor considering stator anisotropy. *J. Xi'an Jiaotong Univ.* **2017**, *51*, 60–68.
5. Lin, F.; Zuo, S.G.; Deng, W.Z. Modeling and Analysis of Electromagnetic Force, Vibration and Noise in Permanent Magnet Synchronous Motor Considering Current Harmonics. *IEEE Trans. Ind. Electron.* **2016**, *63*, 7455–7466.
6. Mehrgou, M.; Pohn, J.; Graf, B. Advanced CAE Methods for NVH Development of High-Speed Electric Axle. In Proceedings of the 11th International Styrian Noise, Vibration & Harshness Congress: The European Automotive Noise Conference, Graz, Austria, 17–19 June 2020.
7. Wang, Y.; Hao, Z.Y.; Zheng, K.; Zheng, X.; Qiu, Y. Analysis of electromagnetic noise of permanent magnet synchronous motor based on multi-directional electromagnetic force. *J. Zhejiang Univ.* **2020**, *54*, 2286–2293.
8. Zhang, L.J.; Xu, J.; Meng, D.J. Effect of tangential electromagnetic force on electromagnetic vibration of permanent magnet synchronous in-wheel motor. *J. Tongji Univ.* **2019**, *47*, 126–132.
9. Bogdevičius, M.; Karpenko, M.; Bogdevičius, P. Determination of rheological model coefficients of pipeline composite material layers based on spectrum analysis and optimization. *J. Theor. Appl. Mech.* **2021**, *59*, 265–278. [CrossRef]

10. Xiaohua, L.; Rongjian, Z.; Xiaotong, T.; Nenghong, X.; Wendan, H. Study on vibration and noise characteristics of interior permanent magnet synchronous machine for electric vehicles by inverter. *Trans. China Electrotech. Soc.* **2020**, *35*, 4455–4464.
11. Han, X.Y.; Li, C.L.; Zhang, X.G. Quasi-analytical calculation of vibration and noise of permanent magnet assisted synchronous reluctance motor and analysis of its influencing factors. *Electri C Mach. Control.* **2020**, *24*, 1–8.
12. He, Y.S.; Zhou, Q.Z.; Zhao, Q. Numerical Simulation on the Electromagnetic Noise of a Vehicle Alternator. *Automot. Eng.* **2017**, *39*, 1198–1202.
13. Dupont, J.; Aydoun, R.; Bouvet, P. Simulation of the Noise Radiated by an Automotive Electric Motor: Influence of the Motor Defects. *SAE Int. J. Altern. Powertrains* **2014**, *3*, 310–320. [CrossRef]
14. Xu, K.; Ying, H.L.; Huang, S.R. Electromagnetic noise reduction of permanent magnet synchronous motor by step-skewed rotor. *J. Zhejiang Univ.* **2019**, *53*, 2248–2254.
15. Wang, X.Y.; He, X.Y.; Gao, P. Research on electromagnetic vibration and noise reduction method of V type magnet rotor permanent magnet motor electric vehicles. *Proc. CSEE* **2019**, *39*, 4919–4926+4994.
16. Park, J.; Lee, H. Study on the Vehicle Cabin Noise Employing the Interfacial Friction in Double Layered Frames Used in Electric Vehicle Traction Motors. *J. Passeng. Cars Electron. Electr. Syst.* **2013**, *7*, 28–35. [CrossRef]
17. Yang, H.D.; Chen, Y.S. Electromagnetic Vibration Analysis and Suppression of Permanent Magnet Synchronous Motor with Fractional Slot Combination. *Proc. CSEE* **2011**, *31*, 83–89.
18. Xie, Y.; Li, F.; Li, Z.W. Optimized Design and Research of Vibration Reduction with an Interior Permanent Magnet Synchronous Motor. *Proc. CSEE* **2017**, *37*, 5437–5445+5543.
19. Jin, M.; Fei, W.; Shen, J. Investigation of Axial Magnetic Force in Permanent Magnet Synchronous Machines with Rotor Step Skewing. *Trans. China Electrotech. Soc.* **2013**, *28*, 19–27.
20. Islam, R.; Husain, I. Analytical Model for Predicting Noise and Vibration in Permanent Magnet Synchronous Motors. *IEEE Trans. Ind. Appl.* **2010**, *46*, 2346–2354. [CrossRef]
21. Song, Z.; Yu, Y.; Chai, F. Radial Force and Vibration Calculation for Modular Permanent Magnet Synchronous Machine with Symmetrical and Asymmetrical Open-Circuit Faults. *IEEE Trans. Magn.* **2018**, *54*, 1–5. [CrossRef]
22. Zuo, S.G.; Zhang, Y.D.; Yan, J. The values of these material parameters in the article were taken with reference to some existing literature. *J. Xi'an Jiaotong Univ.* **2017**, *51*, 60–68.
23. Li, X.H.; Liu, C.J.; Mei, B.S. Vibration and Noise Sources Analysis of IPMSM for Electric Vehicles in a Wide-speed Range. *Proc. CSEE* **2018**, *17*, 5219–5227.